sciendo

Research Note • DOI: 10.2478/gsr-2020-0004 GSR • 8 • 2020 • 31–44

Gravitational and Space Research

Omni-Gravity Nanophotonic Heating and Leidenfrost-Driven Water Recovery System

Rawand M. Rasheed[1,2], Evan A. Thomas[3], Paul Gardner[4], Tanya Rogers[2], Rafael Verduzco[2], Mark M. Weislogel[1]

[1]Portland State University, Portland , OR; [2]Department of Mechanical Engineering, Rice University, Houston, TX; [3]University of Colorado Boulder, Boulder, CO; [4]Shear Development, Portland, OR

Abstract

Recycling systems aboard spacecraft are currently limited to approximately 80% water recovery from urine. To address challenges associated with odors, contamination, and microgravity fluid flow phenomena, current systems use toxic pretreatment chemicals, filters, and rotary separators. Herein, a semipassive and potentially contaminant- and biofouling-free approach to spacecraft urine processing is developed by combining passive liquid–gas separation, nanophotonic pasteurization, and noncontact Leidenfrost droplet distillation. The system aims to achieve >98% water recovery from wastewater streams in zero, Lunar, Martian, and terrestrial gravitational environments. The surfaces of the phase separator are coated with carbon black nanoparticles that are irradiated by infrared light-emitting diodes (LEDs) producing hyperlocal heating and pasteurization during urine collection, separation, and storage. For the prescribed flow rate and timeline, the urine is then introduced into a heated 8.5-m-long helical hemicircular aluminum track. The low pitch and the high temperature of the track combine to establish weakly gravity-driven noncontact Leidenfrost droplet distillation conditions. In our technology demonstrations, salt-free distillate and concentrated brine are successfully recovered from saltwater feed stocks. We estimate equivalent system mass metrics for the approach, which compare favorably to the current water recovery system aboard the International Space Station.

Keywords

Leidenfrost • Superhydrophobic • Life support • Urine water recovery • Omni-gravity • Noncontact distillation

INTRODUCTION

Present spacecraft water recovery technologies are susceptible to fouling and failures due to biological and mineral scaling (Carter, 2010; Wong et al., 2010; Carter et al., 2013). Such failures require expensive and time-consuming maintenance and resupply and are thus limited to spacecraft where such resources are available (Pruitt et al., 2015). Long-duration spaceflight missions, such as extended stays at Lunar outposts or during Mars transit, will increasingly benefit from water recovery equipment that minimizes the impact of fouling. Such systems would also benefit from a minimization of moving parts, energy usage, and maintenance requirements. In this work, capillary solutions are used in conjunction with nanophotonic hyperlocalized heating to promote fouling-free fluid management at all gravity levels. Our target application concerns urine water recovery aboard spacecraft where we uniquely exploit Leidenfrost (Leidenfrost, 1756) droplet levitation due to the underside evaporation layer to achieve noncontact heat-driven distillation with expectations of >98% water recovery. Figure 1 presents a model of the system with passive phase separator (PPS), nanophotonic surfaces, and Leidenfrost distiller identified; and Figure 2 presents a block diagram representation of the system process.

Passive Capillary Phase Separation

Capillary fluid management systems have been exploited aboard spacecraft for decades. These systems typically use clean, single-component fluids, such as fuels, cryogens, and thermal fluids for which the wetting conditions are known and favorable, with contact angles θ generally close to 0°. However, for aqueous mixtures of life support fluids, poor, variable, or even unknown wetting conditions ($0° < \theta < 120°$) are common. As a result, capillary solutions have historically been neglected for spacecraft water-based systems. Instead, forced flows and rotary separation devices have been used to perform essential fluid phase separations (Weislogel et al., 2009). Such engineering solutions using dynamic system components (e.g., rotary separators) are potentially unfavorable due to increased power consumption, failure modes, system complexity, and

†Corresponding author: Rawand M. Rasheed
E-mail: rawand@rice.edu

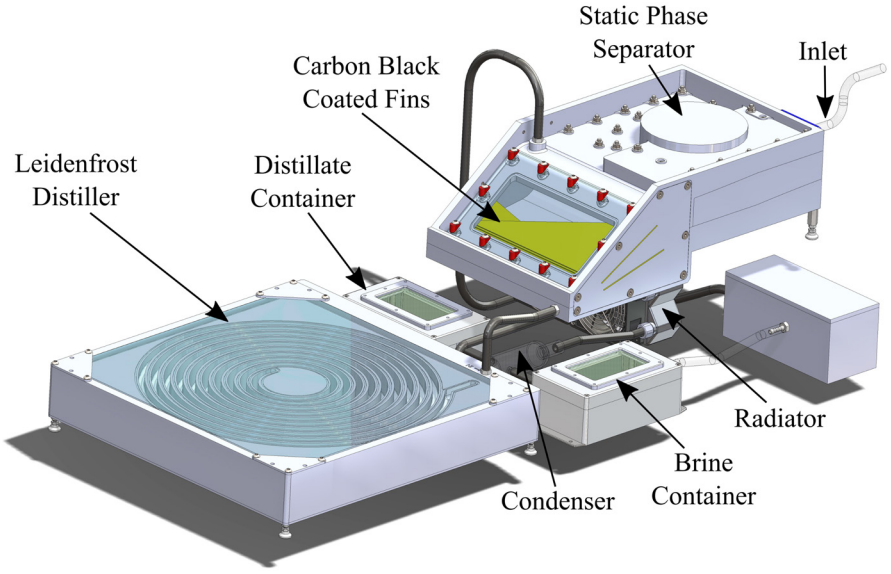

Figure 1. Solid model of water recovery system with components labeled. The dimensions of the Leidenfrost Distiller and PPS are 24″×24″×4″ and 12″×8″×24″, respectively.

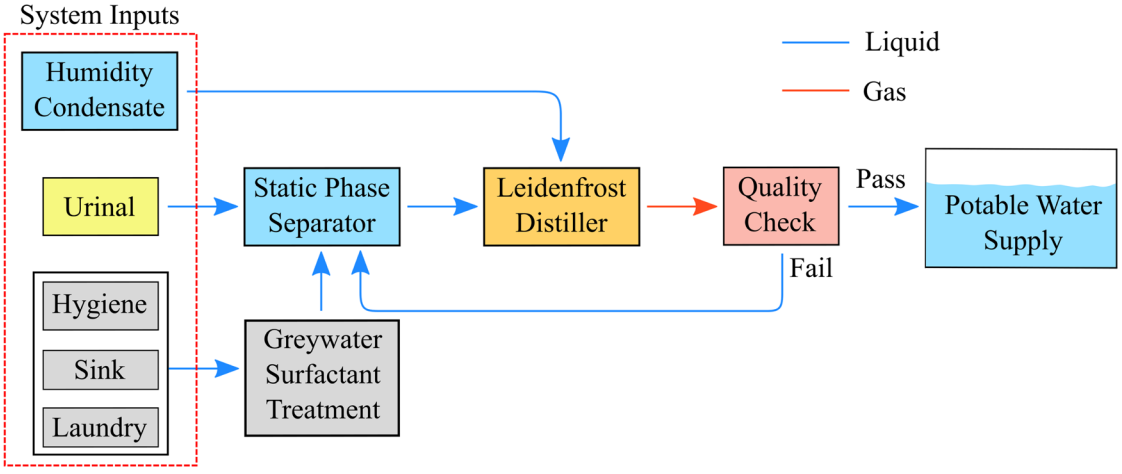

Figure 2. Block diagram of the model in Figure 1.

noise (Johnson, 2002). Exploiting passive capillary forces, even when wetting conditions are not ideal, provides the potential for reducing moving parts, power consumption, and noise while increasing reliability. For example, low-gravity phase separators that use overlapping geometric capillary solutions to convert droplet streams to separate gas–liquid fractions have been developed and demonstrated (Weislogel et al., 2009, 2011). Such systems can accommodate unfavorable wetting conditions and achieve nearly 100% separation for fluids of widely varying contact angles (Thomas and Muirhead, 2009; Thomas et al., 2010). Herein, a PPS, also called a static phase separator, is utilized for separation of the liquid and gas phases in microgravity- and gravity-dominated environments.

Pasteurization

Nanophotonic heating may be exploited for the pasteurization of wastewater directly within the PPS. As an example, when spherical nanoparticles (i.e., gold or carbon) interact with a specific wavelength of light, the nanoparticles experience a harmonic shift in electron polarity, causing the particle to resonate, thus creating a localized heating effect over distances of approximately 10 μm (Richardson et al., 2009). This phenomenon is known as surface plasmon resonance

(Agrawal et al., 2018). Hogan et al. (2014) demonstrate both localized heating and steam generation in a water bath without significant heating of the bulk solution by using light-induced localized heating of dispersed nanoparticles. In such a regime, light is both scattered and absorbed, concentrating electromagnetic energy in a small volume. Neumann et al. (2012) demonstrate this effect using solar light. Such light-induced heating of nanoparticles has gained significant attention in the past decade (Zhang et al., 2006; Pattani and Tunnell, 2012; Bora et al., 2016) for applications in localized drug delivery (Niikura et al., 2013), cancer treatment (Lee et al., 2010; Zhang et al., 2013), saltwater distillation (Dongare et al., 2017), and others (Govorov et al., 2006; de Aberasturi et al., 2015). Herein, we use infrared (IR) light-emitting diode (LED)-induced localized heating of carbon black nanoparticles. For batch operations, our system may require the temporary storage of wastewater, which must be maintained at elevated temperatures to discourage biofouling. Thus, our nanophotonic heating approach is designed for the pasteurization of wastewater. We demonstrate the approach with saltwater.

Leidenfrost Distillation

The enhanced microgravity Leidenfrost phenomenon can be exploited to promote heat-driven noncontact distillation of wastewater droplet streams. On earth, heat-driven distillation is typically used in the pooling boiling regime to perform distillation of liquid–liquid and liquid–solute solutions. Liquid droplets undergo pool boiling when deposited on substrates at or slightly above the liquid's boiling temperature. In this regime, wall-bound droplets undergo nucleate boiling and boil away in seconds. However, if the liquid droplets are deposited on a substrate with a temperature significantly higher than the liquid's boiling temperature, the droplets do not undergo nucleate boiling but will instead levitate on their own vapor layer. The droplets are insulated from the heated substrate by this vapor layer, reducing heat transfer to the droplets by orders of magnitude and eliminating nucleation sites for bubble formation. These combined effects significantly increase droplet lifetimes. For example, capillary-sized droplets of water (< 0.08 mL) deposited on an aluminum substrate held at the Leidenfrost point of water on aluminum (193°C) will require several minutes to evaporate completely.

Leidenfrost phenomenon is enhanced and occurs over significantly larger length scales in the near-weightless microgravity environment. As shown in Fig. 3 a series of images during a drop tower experiment demonstrate this point where ethanol droplets 2.6 mm in diameter are injected into a glass U-tube above the dynamic Leidenfrost point of ethanol on glass (>360°C). The noncontact nature of the phenomenon is attractive as a potentially fouling-free mechanism for distillation aboard spacecraft. Since Leidenfrost distillation is a heat-driven process, complete distillation of wastewater droplets to their salty constituents is possible. The streams of vapor-insulated Leidenfrost droplets are highly mobile and readily circulated using bulk air flows or the evaporating droplets' own vapor pressure.

Stamey and Mihara (1980) present the experimental results for bacterial growth in sterile urine from human subjects, finding that exponential bacterial growth occurs after 2 h for many types of bacteria. Leidenfrost distillation rates are comparable to human urine delivery rates (minutes), which permits essentially real-time distillation of streams of droplets at elevated temperatures before bacterial contamination can occur. Such rapid distillation of urine at temperatures >70°C retards microbial growth, thus reducing or eliminating the need for using urine pretreatment chemicals to prevent bacterial growth in urine in current spacecraft water recovery equipment.

The Leidenfrost effect has been studied extensively for its relevance to numerous applications, including metal manufacturing, fuel combustion, jet and rocket engine propulsion, spray cooling, nuclear reactor cooling, and others (Itaru and Kunihide, 1978; Avedisian and Koplik, 1987; Bernardin et al., 1997; Rein, 2002; Abramzon and Sazhin, 2005; Tarozzi et al., 2007; Sazhin et al., 2010; Gradeck et al., 2011; Wu and Sirignano, 2011). The progression of a particularly applicable line of research has led to the extreme enhancement of Leidenfrost phenomena in microgravity using superhydrophobic (SH) substrates (Biance et al., 2003; Vakarelski et al., 2012; Orzechowski and Wciślik, 2014; Maquet et al., 2015; Attari et al., 2016; Wollman et al., 2016; Rasheed and Weislogel, 2019a; Rasheed and Weislogel, 2019b; Rasheed, 2019). Though our intended application requires a reduced-gravity environment, our reported research is limited to terrestrial demonstrations.

DEVELOPMENT OF WASTEWATER RECOVERY SYSTEM

The omni-gravity nanophotonic heating and Leidenfrost-driven fouling-free water recovery system (WRS), pictured in Figure 1, is a two-loop system capable of continuous processing of wastewater at a rate of 500 mL/h. The processing rate is selected to accommodate the production rates of a crew of four (assuming 1.5 L/d per crew member; Chiaramonte and Joshi, 2004). The block diagram of Figure 2 remains the same for the WRS in all gravity environments, though specific unit geometries may vary. Wastewater streams aboard spacecraft typically comprise humid cabin air condensate (respiration and perspiration), urine, and gray water sources (hygiene, sink, and laundry). Humidity condensates are typically collected

Figure 3. Figure shows 17-Hz images of a pressure-driven ethanol jet producing 2.6-mm droplets at an average velocity of 22 cm/s from a 20-gauge needle injected into a 4.0 mm inner diameter, 63-mm-long glass U-tube.

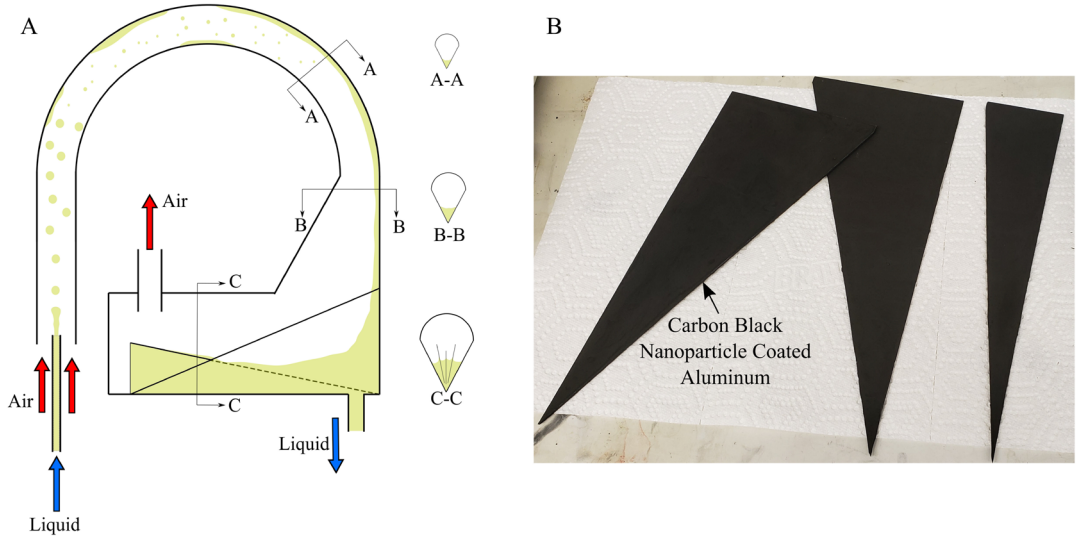

Figure 4. (a) Schematic of the passive phase separator (PPS). Separation of liquid–gas streams in microgravity is achieved utilizing centrifugal forces to promote droplet collisions onto surfaces. Liquid is then wicked into and driven along the interior corners. (b) Aluminum vanes coated with carbon black nanoparticles for insertion into PPS (refer Figure 5).

by condensing heat exchangers and are sufficiently sterile to be directly distilled. For this approach, humidity condensates may be sent directly to the Leidenfrost distiller, as shown in Figure 2. Urine and gray water are delivered to the distiller from the PPS. The distiller is designed to process streams at a rate of up to 500 mL/h. The PPS has a capacity of 1 L for separation and storage. The distiller outlet stream is checked for quality and reprocessed until adequate.

Liquid–Gas Static Phase Separator Design

The PPS device geometry was previously developed and tested in a low-*g* environment demonstrating successful liquid–gas phase separation under highly variable wetting conditions (Weislogel et al., 2009). In this work, we apply scaling laws to the flight-demonstrated subscale model to develop a full-scale PPS capable of collecting, separating, and storing up to 1 L of liquid in zero-gravity and partial-gravity environments such as the moon or Mars. Figure 4 provides a schematic of the PPS with cross sections provided at key locations. In microgravity, wastewater streams enter the PPS and traverse a series of loops, inducing modest centrifugal forces on the droplet stream, causing droplets to collide with the walls of the device. Cross-sectional interior corner geometries in the PPS cause the wetting fluids ($\theta < 90°$) to wick into the interior corner. Capillary forces hold the fluid in the interior corner. A capillary gradient resulting from the varied interior corner half-angle (cross sections A–A to B–B) and the veined structures (cross section C–C) at the PPS outlet induce a stable separated flow that guides the fluid downstream to the PPS outlet.

In gravity-dominated environments, the separation of liquid–gas streams in the PPS is accomplished predominantly by buoyancy. The interior core of the PPS is designed with a 5° tilt with respect to the gravitation vector. The tilt does not affect the microgravity performance but provides for gravity draining of the liquid from the PPS inlet to the finned PPS reservoir, as shown in Figure 5. For the same purpose, the vaned reservoir is sloped at 30° to promote fluid containment in a gravitational environment. Figure

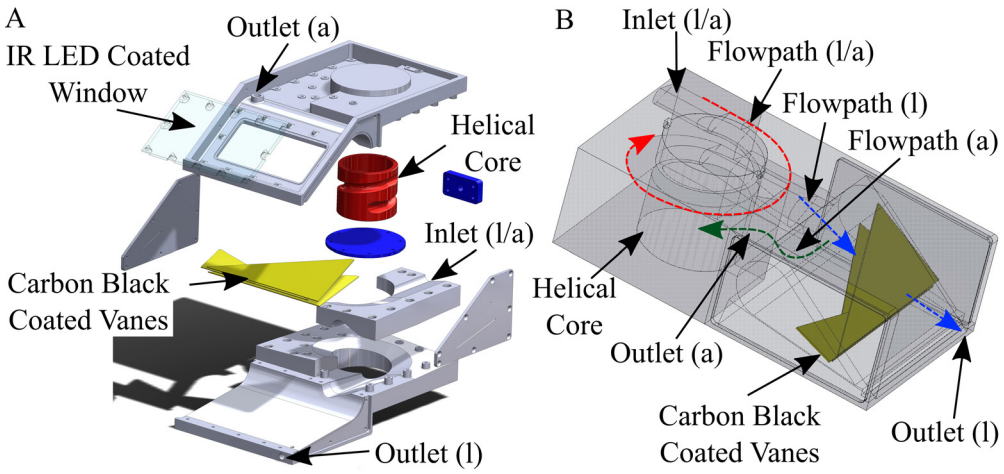

Figure 5. (a) Solid model exploded view of PPS. Gray components are aluminum, yellow capillary vanes are carbon black-coated aluminum, and the red helical core is 3D printed PLA. (b) Solid model of the assembled PPS rotated 90°, with sketch of the flow path. The letters (l) and (a) denote liquid and air, respectively.

5b presents a computer-aided design (CAD) rendering of the assembled PPS. The multicomponent device consists of a helical coiled teardrop sectioned core, which expands into a vaned capillary collection and containment/reservoir section. As demonstrated by Weislogel et al. (2009), and as depicted in Figure 4a, for an intermittent jet and droplet-laden airflow, the helical entrance region provides for the passive low-*g* formation of a separated, collected, and guided rivulet flow regardless of wetting conditions such that a single connected liquid stream is fed into the vaned reservoir, where it is contained by capillary forces. The PPS body is made primarily of aluminum (Figure 5a, gray and blue components). The reservoir vanes (Figure 5a, yellow component) are made of carbon black-coated aluminum, and the helical coil core (Figure 5a red) is made from three-dimensional (3D) printed polylactide (PLA). In a similar manner to liquid management devices for spacecraft fuel tanks (Hartwig, 2016), these vanes further divide the primary interior corner of the teardrop cross-sectioned reservoir into narrower interior corners for greater wicking into the vertices of the reservoir and greater stability. The PPS has a glass window, where IR LEDs are mounted to irradiate the carbon black nanoparticles on the vanes.

Carbon Black Nanoparticle Coating

The triangular aluminum vanes (shown in Figures 4b and 5) are made of 2.5-mm-thick aluminum and coated with carbon black nanoparticles deposited by a plasmonic nanoparticle solution. Activated carbon (CEP21K; surface area 2040 m^2/g) was purchased from Power Carbon Technology Co., Ltd. Gold nanoparticles (AuNPs) of 15-nm outer diameter (OD) suspended in 0.1 mM phosphate-buffered saline (PBS) was purchased from Sigma-Aldrich. Fully hydrolyzed poly(vinyl alcohol) (PVA; molecular weight = 89,000–98,000 g/mol) and 25 wt% aqueous solution of glutaraldehyde (GA) were purchased from Sigma-Aldrich.

The solution for treatment of plasmonic nanoparticle surfaces was composed of 70 wt% of high-surface-area powdered activated carbon (PAC), 20 wt% of 15-nm AuNPs in PBS, and 10 wt% of polymeric binder (linear polymer PVA and cross-linker GA) based on total mass. First, 6 wt% PVA solution was prepared by mixing PVA in deionized (DI) water at 90°C for 4 h. Next, 5 mol% (relative to PVA repeat units) of GA solution was added and mixed for 1 h. PAC was added slowly along with additional DI water, giving a solid content of the solution of approximately 30 wt%. The resulting mixture was stirred for 12 h to ensure solution homogeneity. Lastly, 20 wt% of AuNPs was added to the solution and allowed to mix for an additional hour. In total, 6 mL of nanoparticle solution was manually flow-coated onto each aluminum fin. A pipette was used to deposit the solution across the fin surface and then spread into a thin film using an acrylic planar surface. The vanes were allowed to dry at room temperature and then placed in an oven at 130°C for 1 h to cross-link. The aluminum vanes coated with carbon black nanoparticles are shown in Figure 4b. Partially wetting states with water are achieved on such surfaces, the contact angles in this case being $\theta < 90°$.

Noncontact Leidenfrost Distiller Design

The Leidenfrost distiller is a gravity-sensitive device that must account for adequate droplet residence time to complete the desired distillation. If residence times are too long, complete droplet distillation is achieved before exiting the distiller, potentially resulting in fouling of the distiller surfaces with precipitates. If too short, the droplets may be insufficiently

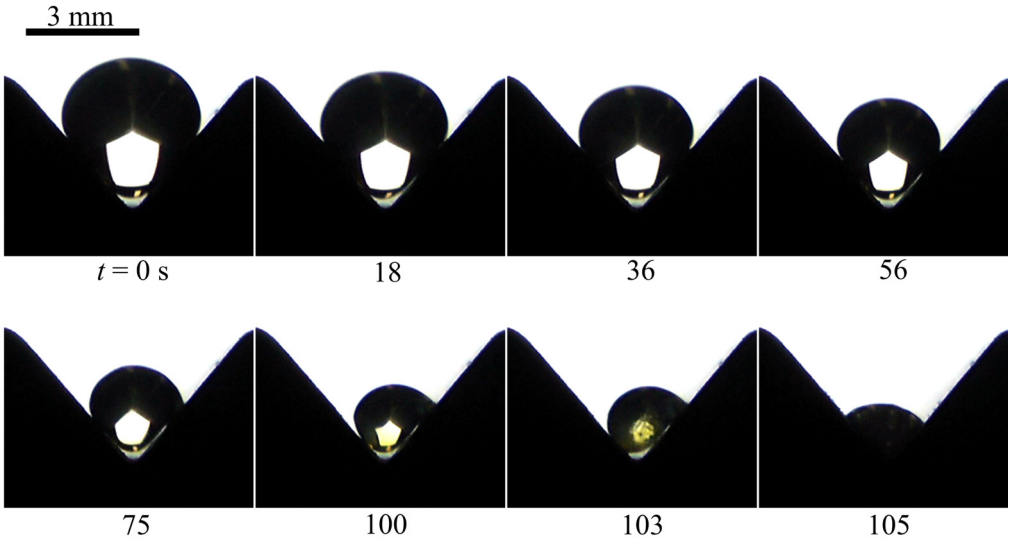

Figure 6. A droplet of urine, 2.0 mm in radius, distilled on a 90° grooved SH plate held at 140°C. A wetting transition is observed between t = 100 and 103 s, where the droplet radius is reduced below 0.9 mm—an approximately 92% reduction in volume.

distilled and must be either remixed and recirculated through the device or must be postprocessed. For our highly aqueous solutions, ≈ 90% droplet distillation in the Leidenfrost distiller is chosen, which significantly distills the droplets while protecting the distiller surfaces from potential fouling due to the precipitation of solutes in wastewater solutions. Passive, postprocess evaporation in a heated, disposable catch basin performs the remainder of the distillation. Figure 6 shows a series of images of a urine droplet distilled on a SH surface held at 140°C, which is above the Leidenfrost point for this wetting condition. After approximately 92% droplet distillation, the solutes in urine begin to precipitate, changing the urine composition from predominantly water-based to oil-based. Oily solutions have drastically lower surface tension values than water, resulting in dramatically elevated Leidenfrost point temperatures relative to water (Chen et al., 2018). This transition is shown in Figure 6 at t = 100 s and t = 103 s, where the droplet first wets and fouls the SH surface. The distiller may be tuned for this specific fluid. For example, this Leidenfrost distiller requires the balance of surface temperature and pitch: the temperature dictates the droplet distillation rate, and the pitch determines the droplet velocity (distiller length) and thus residence time.

Droplet evaporation rates are predicted from a simple mathematical model adopted to size the system, which characterizes the heat transfer from a hot surface to a droplet on a surface above the Leidenfrost temperature. Figure 7 provides a schematic of a droplet with time-varying radius $r(t)$ at saturation temperature T_d rolling with linear velocity u on a superheated surface with temperature T_s and tilt angle α in an ambient environment with temperature T_∞. Through a balance between the hydrostatic pressure from the droplet mass and the vapor pressure from the droplet evaporation, a scale expression for the Leidenfrost vapor layer thickness is derived:

$$\delta \sim \left(\frac{\mu_v k_v \Delta T_1}{2\rho_l \rho_v g(c_p \Delta T_2 + h_{fg})}\right)^{1/3} \quad (1)$$

where k_v (W/mK) is the thermal conductivity of the droplet vapor, ρ_l (kg/m^3) is the liquid droplet density, ρ_v (kg/m^3) is the droplet vapor density, μ_v (Pa-s) is the droplet vapor viscosity, c_p (J/kg·K) is the droplet specific heat, h_{fg} (J/kg) is the droplet latent heat of vaporization, g (m/s^2) is the gravitational acceleration, $\Delta T_1 = T_s - T_d$ is the difference between plate temperature and droplet saturation temperature, and $\Delta T_2 = T_d - T_o$ is the difference between droplet saturation temperature and initial droplet temperature. For simplicity in our sizing calculations, we assume average constant fluid properties. Further, assuming a planar droplet surface at the droplet substrate interface and balancing the vapor pressure with the viscous forces where the vapor pressure is expressed in terms of the droplet hydrostatic pressure, a scale expression for the vapor velocity is derived: $u_{vap} \sim (2_{\rho l}\, g\delta^2)/\mu_v$. The Reynolds number $\mathrm{Re} = (\rho_l u_{vap} \delta)/\mu_v$ is computed for the vapor flow, and suggests laminar flow in the vapor layer. Assuming constant planar substrate temperature with an insulated boundary condition, the Nusselt number is constant and approximately equal to 4.86 (Ramadhyani et al., 1985). Using Eq. (1) and setting the droplet heat transfer area equal to the projected spherical cap area at ≈ 90% of the droplet radius, the steady thin film convection through the vapor layer to the droplet can then be expressed as follows:

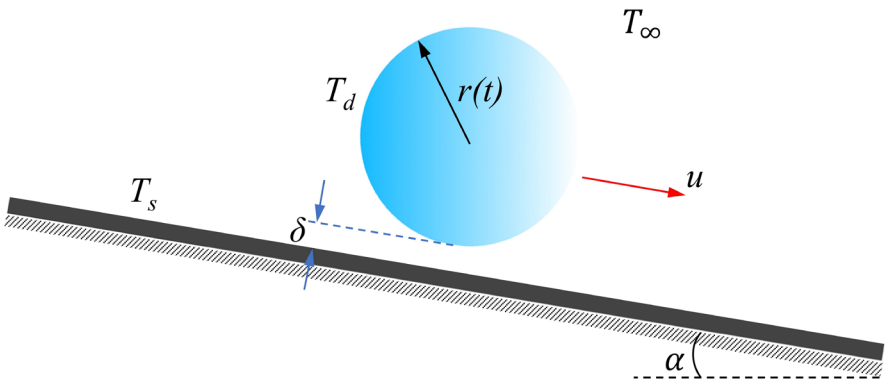

Figure 7. A droplet rolling with linear velocity *u* on a heated tilted substrate exceeding the liquid's Leidenfrost point.

$$q \approx \pi r^2 (k_v \Delta T_1)^{2/3} \left(2\rho_l \rho_v g \left(c_p \Delta T_2 + h_{fg}\right) \mu_v^{-1}\right)^{1/3}. \quad (2)$$

Order of magnitude comparisons show that thin film convection is the dominant mode of heat transfer to the droplet, while the magnitudes of the outer region's forced convection, free convection, and radiation are small. Forced outer region convection over the spherical drops may be considered (Rasheed and Weislogel, 2019b), but for the operating conditions of the Leidenfrost distiller device here, the magnitude of spherical drop forced convection is also small. The rate of change of mass for an evaporating spherical droplet can be expressed as

$$\dot{m} = -4\pi\rho_l r^2 r_t, \quad (3)$$

where $r_t \equiv dr/dt$ is the rate of change of the droplet radius with respect to time. The flow rate of the evaporative mass is expressed in terms of the total heat transfer to the droplet using the expression $q = \dot{m}(c_p \Delta T_2 + h_{fg})$; substitution of Eqs (2) and (3) into this equation results in a first-order linear ordinary differential equation describing the droplet evaporation rate:

$$r_t = \frac{1}{4}\left(\frac{k_v \Delta T_1}{\rho_l \sqrt{\mu_v}(c_p \Delta T_2 + h_{fg})}\right)^{2/3} (2\rho_v g)^{1/3}. \quad (4)$$

Integration of Eq. (4) with $r(t=0) = R_o$ results in

$$r(t) = R_o - kt, \quad (5)$$

where

$$k \equiv \frac{1}{4}\left(\frac{k_v \Delta T_1}{\rho_l \sqrt{\mu_v}(c_p \Delta T_2 + h_{fg})}\right)^{2/3} (2\rho_v g)^{1/3}.$$

Table 1. Sample values used to compute residence time.

T_d (°C)	T_s (°C)	T_o (°C)	k_v (W/mK)	ρ_l (kg/m³)
100	230	20	29.9E-3	958.3
ρ_v (kg/m³)	μ_v (Pa-s)	c_p (J/kgK)	h_{fg} (J/kg)	k (m/s)
0.49	1.15E-5	4182	2256E3	3.18E-5

Note: Water properties are taken at the saturation temperature (100°C), and vapor properties are taken at the bulk temperature (165°C).

Here, *k* has units of velocity. Solutions to Eq. (5) are used to predict the overall lifetime of a droplet on a surface heated past the Leidenfrost temperature for all levels of gravity.

The Leidenfrost distiller uses a gravity feed for wastewater droplet delivery. Such droplets are typically capillary-sized droplets. The capillary length scale $L_c = (\sigma/\Delta\rho g)^{1/2}$ is established through a balance between the capillary and the gravitational forces. For an aqueous terrestrial system, capillary-sized droplets are typically on the order of 2.7 mm in diameter. To ensure that surfaces remain well above the Leidenfrost point of water on aluminum, the present Leidenfrost distiller is designed to operate at 230°C. Solutions to Eq. (5) for the time to distill 90% of the original water droplet at 230°C suggest a total residence time of approximately 77 s. Table 1 provides the parameter values used to compute the residence time in Eq. (5). To achieve this residence time, a 0.25° pitch hemicircular helical channel of Figure 8 was fabricated. The pitch of the helix was derived equating the gravitational energy with the combined rotational and translational kinetic energy and the air drag. A corresponding total channel length of 8.5 m is required to ensure a droplet residence time of ≈ 75 s in the distiller. Based on the maximum characteristic droplet diameter (≈ 2.7 mm), the channel was milled with a 3/8″ ball nose end mill to achieve the hemicircular channel section shown in Fig. 8b. O-ring grooves were machined as

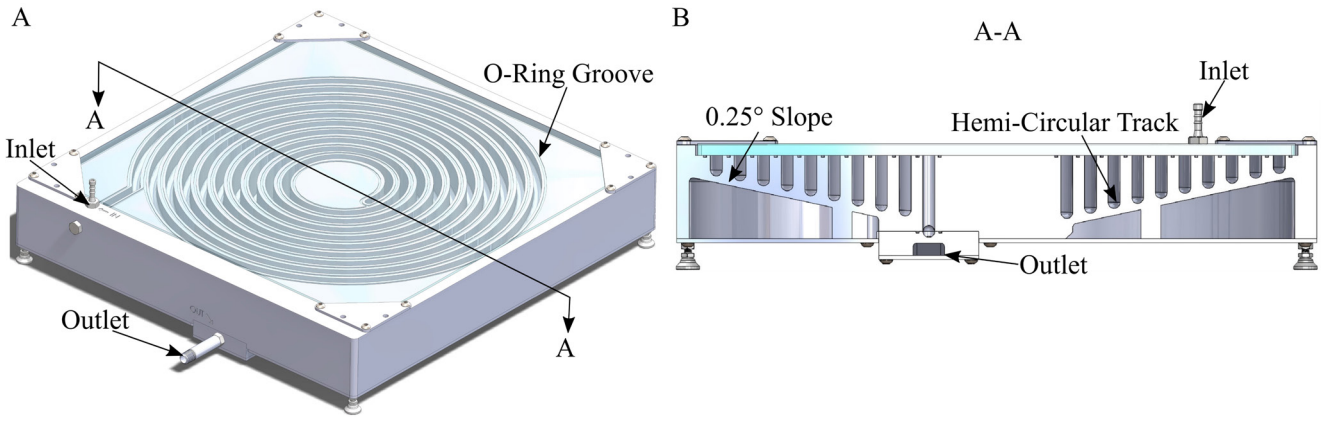

Figure 8. (a) Isometric and (b) section view of the Leidenfrost distiller.

identified for sealing with the 6.35-mm-thick glass lid, clamped with four brackets at each corner of the distiller.

As shown in Eq. (5), the distillation rates in the Leidenfrost state have a weak power law dependence on gravity, but changing the gravitational constant from Earth (1-g_0) to Moon (0.16-g_0) and holding all other parameters constant results in a 170% increase in residence time to achieve 90% distillation of a 2.7-mm droplet. Further, Moon gravity-limited droplet diameters are 244% larger than those on Earth. Gravity-driven droplet velocities are proportional to gravity levels such that lunar velocities are 1/6 those of Earth. The dramatically varying system parameters mean that the present Leidenfrost distiller design is optimized only for a single gravitational environment.

Auxiliary System Components

Other system components include Leidenfrost distiller heaters, heater controls, thermal insulation, a vacuum pump, condenser, and plumbing elements. Figure 9 provides an image of the full system build with labeled components. The distiller heaters consist of two Nichrome resistance heater wires stapled to K23 firebricks. Each heater consists of a wire with 8.4 W nominal resistance capable of dissipating 1440 W per heater wire at 110 V, for a total of approximately 2900 W. This high level of power is required to quickly establish steady state operating temperatures. Once steady conditions are established, the heater power is greatly reduced to approximately 36 W to balance the evaporation rates (≈ 21 W) and losses to the environment (≈ 15 W). A temperature control circuit uses controller, thermocouples, and high-power relays for heater power and temperature set points. The distiller is wrapped in 10-cm-thick high-temperature ceramic fiber insulation to limit losses to the environment.

IR LED (LEDLightsWorld; SMD3528-300-IR) strips of 940-nm nominal wavelength, shown in Figure 9, are used for nanoparticle irradiation. A 200-mm-long jacketed glass coiled reflux condenser is assembled with a Koolance HX-240XC computer cooler capable of ~1700 W cooling (see radiator, cooling fans, and pump; Figure 9). We note that the expeditiously chosen condenser does not account for low-*g* unique phenomena but could if designed by exploiting the geometry solutions identified for the PPS (ref. Figure 5). The vapor products are pumped from the catch basin through the condenser, where they are condensed in a distillate catch basin. The salty droplets are captured and stored in the catch basin. The system is connected, via vacuum tubing, with a vacuum pump inline to draw steam from the distiller to the distillate catch basin.

RESULTS AND DISCUSSION

Nanophotonic Heating

The nanoparticle-coated aluminum vanes were directly exposed to an IR LED source at a peak wavelength of 940 nm. Under the presence of the photon-emitting field, electrons inside the nanoparticles are mobilized as energy carriers through plasmon resonance phenomenon. Excitons are created as heat dissipated through an interband absorption process, both scattering and adsorbing light. The nanoparticles concentrate the light energy into mesoscale volumes near the illuminated fin surface, creating intense localized heating and providing an elevated temperature source for the surrounding mediums. Three case scenarios are tested for localized heating using a SEEK thermal imaging camera. For the baseline scenario, an aluminum coupon was coated with 3 mL of activated carbon CEP21K-H_2O solution, and room temperature readings were recorded. For the second scenario, the coupon was exposed to a 940-nm IR LED strip with a density of 60 LEDs/m placed in a fixed position

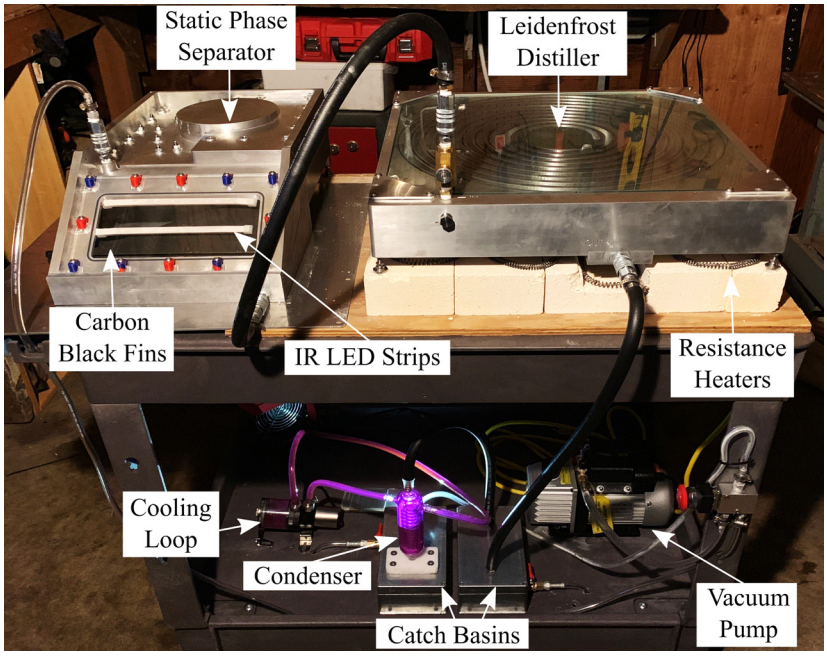

Figure 9. Final water recovery system build with thermal insulation removed.

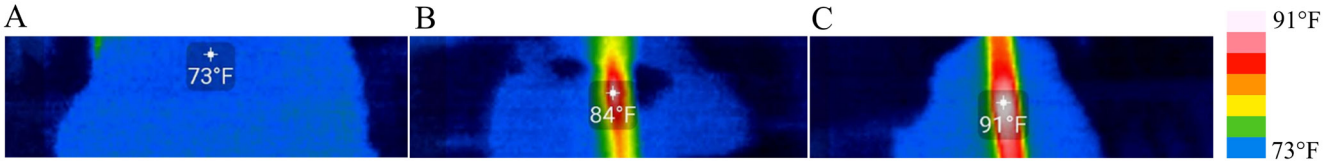

Figure 10. Thermal images from (a) baseline carbon black nanoparticle–aluminum-coated fin at room temperature and (b) exposed to 940-nm IR LED strips with density of 60 LEDs/m. (c) Aluminum vane coated with activated carbon CEP21k-H_2O solution with 20 wt% of 15-nm gold nanoparticle constituent added and exposed to 940-nm IR LED strips with density of 60 LEDs/m. Temperatures in Fahrenheit.

70 mm parallel from the plate surface. Temperature readings were recorded at 1-min intervals until incremental changes were no longer observed after 4 min. For the third scenario, 20 wt% of 15-nm AuNP constituent was added to activated carbon CEP21K-H_2O solution and 3 mL was surface-coated onto a fresh aluminum coupon. The coupon was placed in the same test configuration as Scenario 2.

Figure 10 shows the images highlighting the thermal imaging results for the three test cases. Test coupon 2 (Figure 10b) coated with activated carbon-H_2O solution reached a maximum surface temperature of 28.9°C after 4 min of LED exposure. Test coupon 3 (Figure 10c), which was coated with activated carbon-H_2O and AuNP constituent, reached a maximum surface temperature of 32.8°C after 4 min of exposure. These elevated temperatures, in combination with the biocidal nature of AuNPs (Ravishankar Rai and Jamuna Bai, 2011; Lima et al., 2013) due to the oligodynamic effect, are capable of rendering microbes inactive in both wastewater and recovered distillate streams.

Saltwater Distillation

The Leidenfrost Distiller of Figure 9 was tested at 230°C with saltwater as a urine ersatz fluid. A saltwater salinity of 40 milliSiemens (mS) was chosen to approximate seawater, with similar dissolved solids as urine. The saltwater was supplied to the distiller as a stream of drops, as shown in Figure 11. Distilled salty brine drops were captured in the catch basin (Figure 9). Product steam was pumped to and condensed in the condenser via vacuum pump. All operations were recorded by a high-speed high-density video camera. Deposition of salts on the distiller surfaces was not observed during all the 20 hours of the tests.

The volume and salinity of the distillates and captured brine were measured at different intervals. Figure 12a shows a bar graph of the percent distillate by volume collected. The amount of distillate collected (“water recovery”) was on average ≈ 40% of the total initial influent volume—less than half of the target 90% water recovery rate, for reasons to be discussed shortly. Figure 12b provides a plot of the experimentally measured

evaporation rates of individual droplets measured from videos of distiller experiments at operating temperatures of 230°C and 310°C. Also plotted in Figure 12b are the theoretically determined droplet evaporation rates from Eq. (5), to assess the accuracy of the developed droplet lifetime model. The comparisons of droplet evaporation rates at 230°C indicate good agreement, with an average underprediction of 35%. At 310°C, the underpredictions increase to 54%. We expect that the increased underprediction with increased temperature is due to the increased heating of the droplets from the sidewalls of the channel, which are assumed to be flat for the predictions of Eq. (5).

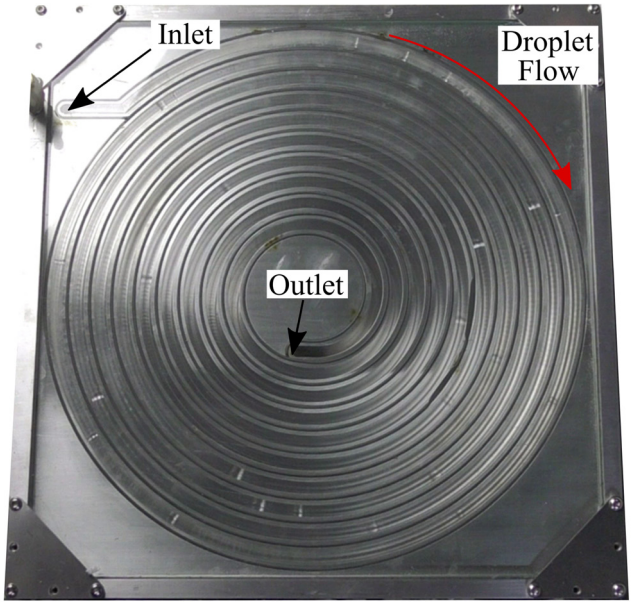

Figure 11. Top view of the Leidenfrost distiller operating at 230°C with droplets of 40 mS saltwater flowing through the distiller.

The model of Eq. (5) provides a conservative estimate for the droplet evaporation rates. The distiller was designed to operate at 230°C for 2.7-mm-diameter droplets with residence time of ≈ 75 s to achieve ≈ 90% distillation. Unfortunately, the residence time achieved was found to be ≈ 30 s, due to the inadvertent enhancement in air/vapor flow caused by the vacuum pump, which could not be avoided. We note that for a constant evaporation rate, nearly 100% (≈ (75/30)*40%) distillation is expected without the enhanced vacuum pump flow. Despite the shortened residence time, the Leidenfrost Distiller performed the distillation function. Figure 13 provides a plot of the measured salinity values for the saltwater influent, captured distillate, and salty brine. The influent was fed to the distiller at a salinity of 40 mS. For all experimental runs, the distillate salinity was measured within instrument error to 0 mS. The average brine salinity was measured to be approximately 58 mS for all experiments, an increase of 45%.

Mass and Energy Trade Analysis

The nanophotonic heating and Leidenfrost-driven fouling-free WRS was evaluated using the equivalent system mass (ESM) metric as developed by Levri et al. (2000) and compared to the current state-of-the-art water recovery technology ESM metrics aboard the International Space Station (ISS). The ISS WRS is a batch process system, whereas the system developed herein is a continuous process system. Both systems, however, are sized to process wastewater streams

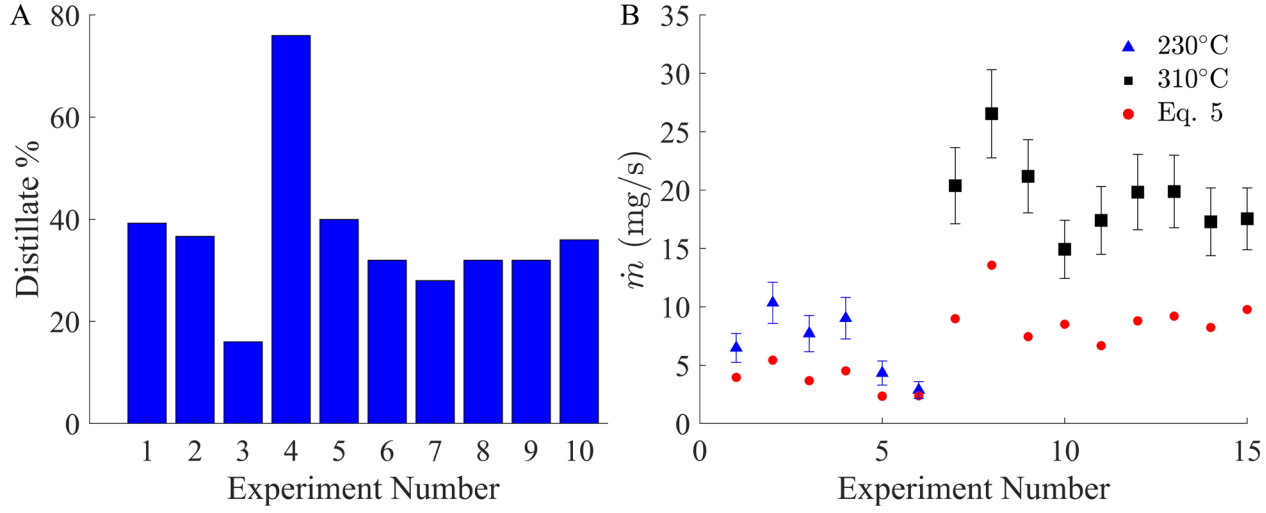

Figure 12. (a) Percent distillate outlet from distiller. (b) Saltwater droplet evaporation rates in distiller at 230°C and 310°C.

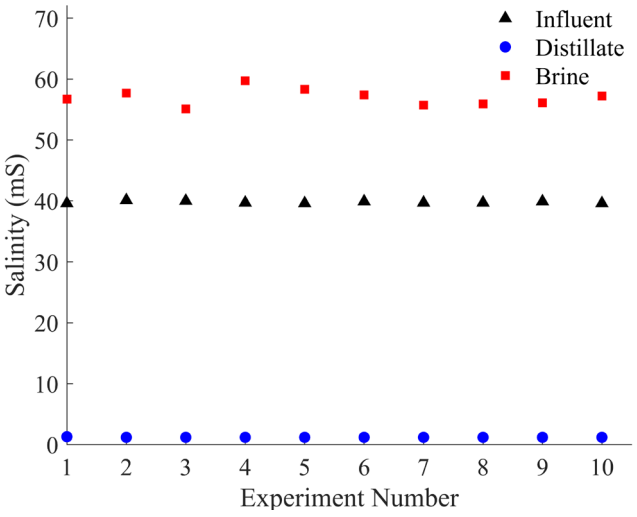

Figure 13. Salinity of the influent saltwater, effluent distillate, and effluent brine at various intervals during Leidenfrost distiller testing.

Table 2. Mass, power, volume, and ESM for ISS WRS and Nanophotonic Heating and Leidenfrost-Driven WRS.

Parameters	ISS WRS	Nanophotonic Heating and Leidenfrost-Driven WRS
Mass (kg)	1380	245
Power (W)	560	650
Volume (m^3)	3.14	0.5
ESM (kg)	1506	392

for a crew of four. A valid ESM comparison can therefore be made to compare the performance of both systems. The ESM metric is an equivalent mass value reflective of a system's mass, volume, and energy requirements and is used when comparing technologies regarding launch and operating costs of a system. The ESM value is computed using the following relationship:

$$\text{ESM} = M + (V * V_{eq}) + (P * P_{eq}) + (C * C_{eq}), \quad (6)$$

where M is the overall system hardware mass in kilograms, V is the system volume in cubic meters, P is the system power requirements in kilowatts (kW), and C is the system cooling power requirement in kW. All aforementioned terms are converted to mass values using infrastructure cost factors V_{eq} (66.66 kg/m^3), P_{eq} (476 kg/kW), and C_{eq} (163.8 kg/kW). The infrastructure cost factors are constant values used to convert system resource requirements to a mass value (Levri et al., 2000). Crew installation and maintenance times are also typically included in ESM trade studies, but in this study, these are assumed to be equivalent for all systems, despite expectations of the present system requiring less maintenance if fouling-free objectives are achieved with fewer consumables, pretreatment chemicals, and moving parts.

Mass and volume values for the present WRS are obtained by summation of the individual component mass measurements and the overall footprint measurements of the system prototype shown in Figure 9. Table 2 lists the mass, power, and volume requirements for the current state-of-the-art WRS aboard the ISS and for the presented Nanophotonic Heating and Leidenfrost-Driven WRS. These metrics are converted to an ESM value and also listed in Table 2. All values for the current state-of-the-art WRS are obtained from the study by Anderson et al. (2018). The Nanophotonic Heating and Leidenfrost-Driven WRS posits an ESM value of 392 kg, which is an attractive value compared to the current state-of-the-art WRS with ESM of 1506 kg. The present WRS fares favorably in terms of mass and volume, with total mass of 245 kg and volume of 0.5 m^3, compared to the current state-of-the-art WRS of 1380 kg and 3.14 m^3, respectively.

Power requirements for the present WRS are computed from the individual system components operating at peak power levels. The 12 VDC flexible IR LED strips consist of 60 LED/m at 940-nm peak wavelength and require 4.8 W/m of power (LEDLightsWorld SMD3528-300-IR). A 1.5-m length of IR LEDs is used, resulting in 7.2 W of power consumption. The vacuum pump requires 208 W, and the condenser cooling loop fans and pump require a total of 60 W. Power consumption of the Leidenfrost distiller is estimated using a thermal resistance model. Assuming a quiescent environment at 20°C, 10 cm of ceramic fiber insulation (k = 0.05 W/mK) and distiller surfaces assumed uniformly held at 230°C results in approximately 15 W of heat loss to the environment. This energy requirement accounts for energy leaking from the system to the ambient environment in the form of radiation, natural convection, and conduction for the Leidenfrost distiller at steady state. For our distillation rate of 8 mg/s (refer Figure 12B) we determine 22 W of power for distillation, and a total steady system power draw of 22 W + 15 W = 37 W.

Distillation of water-based solutions includes the thermal load of sensible heat to heat urine from 20°C to 100°C, and latent heat h_{fgfg} to vaporize the stream; namely, $q = \dot{m}(c_p \Delta T_2 + h_{fg})$, where $\dot{m}$ is the mass flow rate of processed water per hour. For a crew of four, the target rate is 500 mL/h. Thus, the expected energy load is approximately 360 W. Including peripheral power sources and losses yields the expected total power requirements of approximately 650 W.

CONCLUSION

The first omni-gravity WRS utilizing noncontact Leidenfrost distillation and nanophotonic heating as methods to promote fouling-free water recovery from waste streams is

demonstrated herein. An omni-gravity passive liquid–gas phase separator was developed utilizing a helical entrance, expansion, and vaned reservoir to promote the passive separation and containment of wastewater streams despite widely varying or unknown wetting conditions. The device may be vector-oriented to provide this separation and storage function for any gravity environment, especially microgravity. The phase separator surfaces were coated with carbon black nanoparticles that were irradiated with IR LED strips to induce hyperlocal nanophotonic heating to 32.8°C, which promotes and maintains pasteurization of wastewater streams, forestalling microbial growth.

An approximate mathematical model was developed describing droplet evaporation in the Leidenfrost state. The model was then used to design the Leidenfrost distiller. The aluminum distiller was fabricated as a helical hemicircular track ~ 8.5 m in length with 0.25° pitch to establish gravity-driven droplet drainage in a terrestrial environment. The distiller was heated above the Leidenfrost point of water on aluminum via resistance heaters. Tests were performed with 40 mS saltwater as a urine ersatz fluid. Throughout the ~ 20-h operations, no significant salt deposits or other forms of fouling were observed on the distiller surfaces. Volume and salinity measurements over time revealed an average water recovery rate of 40% with virtually no salt content in the recovered distillate, and an average salinity of 58 mS was noted in the captured residual brine. Thus, changes in salinity were consistent with percent distillation recovery. Recovery rates above 90% were predicted for the current design based on droplet residence times of 75 s. However, reduced residence times of only 30 s were achieved in practice due to droplet accelerations arising from an unforeseen vacuum pump assist. We expect that ≈ 90% recovery is readily achievable by reducing the pitch of the helical track.

The present WRS trades favorably with the current state of the art aboard the ISS, with ESM of 392 kg compared to 1506 kg—a nearly four-fold reduction. The nanophotonic Leidenfrost WRS demonstrates the feasibility of an on-demand fouling-free wastewater distillation system with significant reductions in mass, volume, moving parts, caustic consumables, and maintenance requirements. The heat-driven Leidenfrost distillation process boasts the advantage of achieving up to 100% water recovery from wastewater streams. Further development of the approach is recommended.

ACKNOWLEDGMENTS

This work is the result of a collaborative effort supported in part by a NASA Small Business Innovative Research Phase I grant titled “Nanophotonic Capillary Distiller” (80NSSC18P1957), COR John McQuillen, and a NASA Space Technology Research Fellowship grant titled “Leidenfrost Driven Waste-Water Separator” (80NSSC17K0175), September 15, 2017: COR Jennifer Pruitt. We acknowledge key inputs of Dr John C. Graf of the NASA Johnson Space Center.

AUTHOR DISCLOSURE STATEMENT

No competing financial interests exist.

REFERENCES

Abramzon B, Sazhin S (2005) Droplet vaporization model in the presence of thermal radiation. *International Journal of Heat and Mass Transfer* **48**(9), 1868-1873.

Agrawal A, Cho SH, Zandi O, Ghosh S, Johns RW, Milliron DJ. (2018) Localized surface plasmon resonance in semiconductor nanocrystals. *Chemical Reviews* **118**(6), 3121-3207.

Anderson MS, Ewert MK, Keener JF (2018) Life support baseline values and assumptions document.

Attari B, Weislogel M, Wollman A, Chen Y, Snyder T (2016) Puddle jumping: spontaneous ejection of large liquid droplets from hydrophobic surfaces during drop tower tests. *Physics of Fluids* **28**(10), 102104.

Avedisian CT, Koplik J (1987) Leidenfrost boiling of methanol droplets on hot porous/ceramic surfaces. *International Journal of Heat and Mass Transfer* **30**(2), 379-393.

Bernardin JD, Stebbins CJ, Mudawar I (1997) Mapping of impact and heat transfer regimes of water drops impinging on a polished surface. *International Journal of Heat and Mass Transfer* **40**(2), 247-267.

Biance AL, Clanet C, Quéré D (2003) Leidenfrost drops. *Physics of Fluids* **15**(6), 1632-1637.

Bora T, Zoepfl D, Dutta J (2016) Importance of plasmonic heating on visible light driven photocatalysis of gold nanoparticle decorated zinc oxide nanorods. *Scientific Reports* **6**, 26913.

Carter DL, Tobias B, Orozco NY (2013) Status of ISS water management and recovery. In *43rd International Conference on Environmental Systems* (p. 3509).

Carter L (2010, July) Status of the regenerative ECLS water recovery system. In *40th International Conference on Environmental Systems* (p. 6216).

Chen H, Cheng WL, Peng YH, Jiang LJ (2018) Dynamic Leidenfrost temperature increase of impacting droplets containing high-alcohol surfactant. *International Journal of Heat and Mass Transfer* **118**, 1160-1168.

Chiaramonte FP, Joshi JA (2004) Workshop on critical issues in microgravity fluids, transport, and reaction processes in advanced human support technology.

de Aberasturi DJ, Serrano-Montes AB, Liz-Marzán LM (2015) Modern applications of plasmonic nanoparticles: from energy to health. *Advanced Optical Materials* **3**(5), 602-617.

Dongare PD, Alabastri A, Pedersen S, Zodrow KR, Hogan NJ, Neumann O, Wu J, Wang T, Deshmukh A, Elimelech M, Li Q, Nordlander P, Halas NJ (2017) Nanophotonics-enabled solar membrane distillation for off-grid water purification. *Proceedings of the National Academy of Sciences* **114**(27), 6936-6941.

Govorov AO, Zhang W, Skeini T, Richardson H, Lee J, Kotov NA (2006) Gold nanoparticle ensembles as heaters and actuators: melting and collective plasmon resonances. *Nanoscale Research Letters* **1**(1), 84.

Gradeck M, Ouattara A, Maillet D, Gardin P, Lebouché M (2011) Heat transfer associated to a hot surface quenched by a jet of oil-in-water emulsion. *Experimental Thermal and Fluid Science* **35**(5), 841-847.

Hartwig JW (2016) A detailed historical review of propellant management devices for low gravity propellant acquisition. In *52nd AIAA/SAE/ASEE Joint Propulsion Conference,* Salt Lake City, UT, July 25-27, 2016 (p. 4772).

Hogan NJ, Urban AS, Ayala-Orozco C, Pimpinelli A, Nordlander P, Halas NJ (2014) Nanoparticles heat through light localization. *Nano Letters* **14**(8), 4640-4645.

Itaru M, Kunihide M (1978) Heat transfer characteristics of evaporation of a liquid droplet on heated surfaces. *International Journal of Heat and Mass Transfer* **21**(5), 605-613.

Johnson J (2002) Jsc-19935 shuttle ops v08-waste collection system, Houston, TX.

Lee SM, Park H, Yoo KH (2010) Synergistic cancer therapeutic effects of locally delivered drug and heat using multifunctional nanoparticles. *Advanced Materials* **22**(36), 4049-4053.

Leidenfrost JG (1756) On the fixation of water in diverse fire. Transl. C. Wares, 1966. *International Journal of Heat and Mass Transfer* **9**, 1153-1166.

Levri JA, Vaccari DA, Drysdale AE (2000) *Theory and Application of the Equivalent System Mass Metric* (No. 2000-01-2395). SAE Technical Paper.

Lima E, Guerra R, Lara V, Guzmán A (2013) Gold nanoparticles as efficient antimicrobial agents for *Escherichia coli* and *Salmonella typhi*. *Chemistry Central Journal* **7**(1), 11.

Maquet L, Brandenbourger M, Sobac B, Biance AL, Colinet P, Dorbolo S (2015) Leidenfrost drops: effect of gravity. *EPL (Europhysics Letters)* **110**(2), 24001.

Neumann O, Urban AS, Day J, Lal S, Nordlander P, Halas NJ. (2012). Solar vapor generation enabled by nanoparticles. *ACS Nano* **7**(1), 42-49.

Niikura K, Iyo N, Matsuo Y, Mitomo H, Ijiro K (2013) Sub-100 nm gold nanoparticle vesicles as a drug delivery carrier enabling rapid drug release upon light irradiation. *ACS Applied Materials & Interfaces* **5**(9), 3900-3907.

Orzechowski T, Wciślik S. (2014) Analysis of D2-law in case of Leidenfrost drop evaporation. *Experimental Thermal and Fluid Science* **59**, 230-237.

Pattani VP, Tunnell JW (2012) Nanoparticle-mediated photothermal therapy: a comparative study of heating for different particle types. *Lasers in Surgery and Medicine* **44**(8), 675-684.

Pruitt JM, Carter L, Bagdigian RM, Kayatin MJ (2015, July) Upgrades to the ISS water recovery system. In *45th International Conference on Environmental Systems*, Bellevue, Washington, July 12-16, 2015.

Ramadhyani S, Moffatt DF, Incropera FP (1985) Conjugate heat transfer from small isothermal heat sources embedded in a large substrate. *International Journal of Heat and Mass Transfer* **28**(10), 1945-1952.

Rasheed, R. M. (2019). *Non-contact Distillation* (Masters thesis, Portland State University).

Rasheed RM, Weislogel MM (2019a) The unrealized potential of superhydrophobic substrates in advanced life support systems. In *49th International Conference on Environmental Systems*, Boston, Massachusetts, July 7-11, 2019, #224.

Rasheed RM, Weislogel MM (2019b) On-demand non-contact distillation: low-g demonstrations of a Leidenfrost wastewater processor. In *49th International Conference on Environmental Systems*, Boston, Massachusetts, July 7-11, 2019, #222.

Ravishankar Rai V & Jamuna Bai A (2011) Nanoparticles and their potential application as antimicrobials. A Méndez-Vilas A, editor. Mysore: Formatex.

Rein M (2002) Interactions between drops and hot surfaces. In *Drop-Surface Interactions* (pp. 185-217). Vienna: Springer.

Richardson HH, Carlson MT, Tandler PJ, Hernandez P, Govorov AO (2009) Experimental and theoretical studies of light-to-heat conversion and collective heating effects in metal nanoparticle solutions. *Nano Letters* **9**(3), 1139-1146.

Sazhin SS, Krutitskii PA, Gusev IG, Heikal MR (2010) Transient heating of an evaporating droplet. *International Journal of Heat and Mass Transfer* **53**(13-14), 2826-2836.

Stamey TA, Mihara G (1980) Observations on the growth of urethral and vaginal bacteria in sterile urine. *The Journal of Urology* **124**(4), 461-463.

Tarozzi L, Muscio A, Tartarini P (2007) Experimental tests of dropwise cooling on infrared-transparent media. *Experimental Thermal and Fluid Science* **31**(8), 857-865.

Thomas E, Muirhead D (2009) Impact of wastewater fouling on contact angle. *Biofouling* **25**(5), 445-454.

Thomas EA, Weislogel MM, Klaus DM (2010) Design considerations for sustainable spacecraft water management systems. *Advances in Space Research* **46**(6), 761-767.

Vakarelski IU, Patankar NA, Marston JO, Chan DY, Thoroddsen ST (2012) Stabilization of Leidenfrost vapour layer by textured superhydrophobic surfaces. *Nature* **489**(7415), 274.

Weislogel MM, Thomas EA, Graf JC (2009) A novel device addressing design challenges for passive fluid phase separations aboard spacecraft. *Microgravity Science and Technology* **21**(3), 257.

Weislogel MM, Thomas EA, Graf JC (2011) U.S. Patent No. 7,905,946. Washington, DC: U.S. Patent and Trademark Office.

Wollman A, Weislogel M, Wiles B, Pettit D, Snyder T (2016) More investigations in capillary fluidics using a drop tower. *Experiments in Fluids* **57**(4), 57.

Wong WC, Dudinsky LA, Garcia VM, Ott CM, Castro VA (2010) Efficacy of various chemical disinfectants on biofilms formed in spacecraft potable water system components. *Biofouling* **26**(5), 583-586.

Wu G, Sirignano WA (2011) Transient convective burning of interactive fuel droplets in double-layer arrays. *Combustion and Flame* **158**(12), 2395-2407.

Zhang Y, Gu C, Schwartzberg AM, Chen S, Zhang JZ (2006) Optical trapping and light-induced agglomeration of gold nanoparticle aggregates. *Physical Review B* **73**(16), 165405.

Zhang Z, Wang J, Chen C (2013) Near-infrared light-mediated nanoplatforms for cancer thermo-chemotherapy and optical imaging. *Advanced Materials* **25**(28), 3869-3880.